Single-Chain Slip-Link Model of Entangled Polymers: Simultaneous Description of Neutron Spin−Echo, Rheology, and Diffusion

Alexei E. Likhtman*

School of Physics and Astronomy, University of Leeds, Leeds LS2 9JT, UK

Received February 25, 2005; Revised Manuscript Received April 30, 2005

ABSTRACT: The model presented in this paper describes simultaneously three different experimental techniques applied to different monodisperse polymer melts: neutron spin−echo (NSE), linear rheology, and diffusion. First, it shows that the standard tube model cannot be applied to NSE because the statistics of a one-dimensional (1D) chain in a three-dimensional (3D) random-walk tube become wrong on the length scale of the tube diameter, whereas all available NSE data are for scattering vectors in this range. Then a new single-chain dynamic slip-link model on the basis of a recent network model by Rubinstein and Panyukov is introduced. Instead of solving the model analytically, which would require uncontrolled approximations, the model is formulated in terms of stochastic differential equations, suitable for Brownian dynamics simulations. I perform these simple simulations, demonstrate that the model describes individual experiments well, and then compare the results with experiments on monodisperse polyethylene, polyethylene-propylene, polyisoprene, polybutadiene, and polystyrene. For all polymers, model parameters from one experiment are obtained, and the others are predicted without fitting. The results show some systematic discrepancies, suggesting possible inadequacy of the Gaussian chain model for some of the polymers, and possible inadequacy of time−temperature superposition.

1. Introduction

Historically, the theory of polymer dynamics was mainly driven by unique mechanical properties of polymer melts, which are essential for polymer processing applications. The most successful and elegant theory, which was able to predict most qualitative features of rheological behavior, is the tube or reptation theory.[1,2] Because of the success of the tube theory, a growing number of experiments and computer simulations are dedicated to direct and indirect verification of the tube idea. Apart from linear and nonlinear rheology of different molecular architectures, such experiments include neutron scattering, neutron spin−echo (NSE), dielectric spectroscopy, NMR, and self-diffusion measurements.[4,5] There are also significant advances in molecular dynamics simulations,[6−8] which can potentially provide very detailed confirmation of any theory.

However, there is a major problem with most experimental attempts of tube theory verification. Because of the complexity of the modern tube theory, which includes contour length fluctuations and constraint release, almost no experiments can be directly compared with the tube model. Instead, many mathematical and physical approximations are needed to arrive at a formula that can be compared to experiment. Usually, such a formula contains a few fitting parameters, which are adjusted to describe a particular experiment. This approach has two drawbacks. To understand them, one must make a clear distinction between the model and solution of the model, known also as a "theory" or a "fitting formula" to describe the experiment. First, the disagreement between the formula and experiment does not invalidate the model; it is possible that the solution of the model is wrong. It is also possible that the agreement with experiment is a consequence of cancellation of errors of the model and approximations used. And second, because theories for different experiments contain different approximations, the parameters extracted by fitting different experiments may not agree with each other.

In this paper I make an attempt to overcome these two limitations. I propose a new single-chain slip-links model, which is formulated in terms of stochastic equations, suitable for Brownian dynamics simulations. Then, I demonstrate that it is capable of describing all mentioned experiments and does not suffer from internal limitations of the tube model, which are also discussed. Then I focus on simultaneous description of NSE, linear rheology, and diffusion. To avoid complications with mathematical approximations needed to solve this model analytically, I concentrate on simulation results, thus making direct comparison between the model and the experiment. I deliberately stress existing disagreement between the model and experiments, concluding that some elements of this model and other similar models are still missing. Here, I focus on monodisperse linear polymers. However, the model can be easily applied to branched and polydisperse polymers.

2, Current "Standard" Tube Model and NSE

Neutron scattering provides the most detailed and microscopic information about the structure and dynamics of polymer melts. SANS measurements demonstrate that the static structure factor $S(q)$ is not affected by entanglements and is well described by the Debye function, a result of random walk configuration of the chain at all length scales larger than the Kuhn segment. Neutron spin−echo experiments provide a normalized dynamic structure factor in the q-range around the tube diameter and in the time-range around τ_e, the Rouse time of one entanglement segment, roughly described as the time scale when the chain starts to feel the entanglements. The example of such data on hydrogenated polybutadiene (close analogue of polyethylene) is

* Author to whom correspondence should be addressed. E-mail: A.Likhtman@leeds.ac.uk.

10.1021/ma050399h CCC: $30.25
Published on Web 06/14/2005

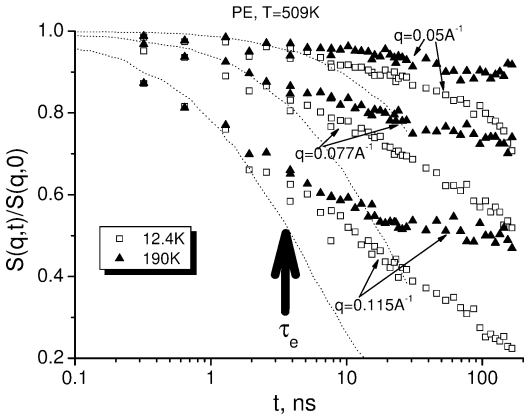

Figure 1. Normalized dynamic structure factor as measured by NSE[14] for two different molecular weights of PEB-2 at three different q-vectors. Dotted lines are predictions of the Rouse theory.

presented on Figure 1 for two molecular weights and three q-vectors. The dotted lines give predictions of the Rouse model. One can see that the early time dynamics are consistent with free Rouse motion, and then, after a few nanoseconds, the dynamics slow down significantly, and for a high-molecular-weight sample, $S(q, t)$ tends to a q-dependent plateau. The chain is completely restricted by entanglements at large length scales (upper curve) and relaxes more as q increases. One also observes that, at late times, the low-molecular-weight sample (which has about 8−10 entanglements) continues relaxing even after τ_e. This relaxation is attributed to contour length fluctuations.[14]

Now we shall try to describe the standard tube model and compare it to the data in Figure 1. The tube model assumes that, at early $t < \tau_e$, the motion of the chain obeys Rouse dynamics, in accordance with experiment. Then, at $t \gg \tau_e$, the motion of the chain obeys one-dimensional (1D) Rouse dynamics in a tube, which is a three-dimensional (3D) random walk with the tube persistence length a equal to its diameter. Then, constraint release is added in some consistent form. The most detailed form of CR was given in ref 9 and combined with the exact solution for 1D Rouse dynamics in ref 19 in the context of linear rheology.

This standard model (without CR) was applied to NSE by de Gennes.[3] To obtain a tractable analytical solution, he considered the case $a \ll 1/q \ll R_g$, where R_g is chain's radius of gyration and a is the tube diameter. We note that the first condition $qa \ll 1$ is not applicable to the data of Figure 1 (and indeed to any literature NSE data) because the tube diameter is estimated to be $a \approx 46$ Å, and therefore, qa is changing from 1.4 to 5.3. However, one may still hope (and indeed been hoping for a long time) that this assumption is not crucial for validity of the theory. In the Appendices A and B, I present solution of the de Gennes model without relying on the assumption $qa \ll 1$. The result of these calculations for the dynamic structure factor is

$$S(q, t) = \frac{12N}{q^2b^2} + \frac{NN_e}{3(1 + q^2a^2/36)}\mathrm{erfc}(\sqrt{t/\hat{\tau}})\exp(t/\hat{\tau}) \quad (1)$$

where

$$\hat{\tau} = \frac{36\pi^2\tau_0}{q^4b^4}$$

and $\tau_0 = \xi b^2/(3\pi^2 k_B T) = 1/(\pi^2 W)$ is the Rouse time of one Kuhn segment (elementary time scale), and W is elementary rate. Here ξ is the friction of one Kuhn segment of size b.

At time $t = 0$, eq 1 gives the static structure factor

$$S(q) = \frac{12N}{q^2b^2} + \frac{NN_e}{3(1 + q^2a^2/36)} \quad (2)$$

which is different from the Debye function, which for $qR_g \gg 1$ is just

$$S_{\mathrm{Debye}}(q) = \frac{12N}{q^2b^2} \quad (3)$$

The result in eq 1 is exactly the same as the de Gennes result apart from the term $(1 + q^2a^2/36)$ in the denominator of the second term. After obtaining this result, de Gennes argued that the first term of eq 1 was calculated without corrections of order qa, and it has to be corrected for that from the condition that the total structure factor must be Debye function eq 3. This would lead to the result

$$S(q, t) = \left(\frac{12N}{q^2b^2} - \frac{NN_e}{3(1 + q^2a^2/36)}\right) + \frac{NN_e}{3(1 + q^2a^2/36)}\mathrm{erfc}(\sqrt{t/\hat{\tau}})\exp(t/\hat{\tau}) \quad (4)$$

If I now omit the term $(1 + q^2a^2/36)$, rearrange the terms in the first part of the expression, and argue that this first constant part must eventually relax by the slower reptation process $\psi_{\mathrm{rep}}(t)$, I arrive at the de Gennes expression

$$S(q, t) = \frac{12N}{q^2b^2}\left(\left(1 - \frac{q^2a^2}{36}\right)\psi_{\mathrm{rep}}(t) + \frac{q^2a^2}{36}\mathrm{erfc}(\sqrt{t/\hat{\tau}})\exp(t/\hat{\tau})\right) \quad (5)$$

where I used $N_e b^2 = a^2$.

This expression, however, gives negative amplitude for the reptation process for $qa > 6$, the fact which lead authors of[26] to replace $(1 - q^2a^2/36)$ by $\exp(-q^2a^2/36)$, arguing that $1 - x$ is just the first term in the Taylor expansion of $\exp(-x)$. Thus, the final expression used to describe NSE experiments for last 10 years was

$$S(q, t) = \frac{12N}{q^2b^2}\left(\exp\left(\frac{q^2a^2}{36}\right)\psi_{\mathrm{rep}}(t) + \left(1 - \exp\left(\frac{q^2a^2}{36}\right)\right)\mathrm{erfc}(\sqrt{t/\hat{\tau}})\exp(t/\hat{\tau})\right) \quad (6)$$

I repeated this derivation here to demonstrate that the formula of eq 6 does not correspond to the tube model described above in the regime $qa \sim 1$ because of the number of unjustified approximations used. Note also that the de Gennes limit $qa \ll 1$ has no practical use because the experimental signal is very close to unity for all times measured. In other words, comparing NSE results with eq 6 is quite different from comparing NSE with the tube model. The main reason the standard tube model is unsuitable for description of NSE experiments is the fact that the static structure factor of a 1D Rouse chain mapped onto a 3D random walk is

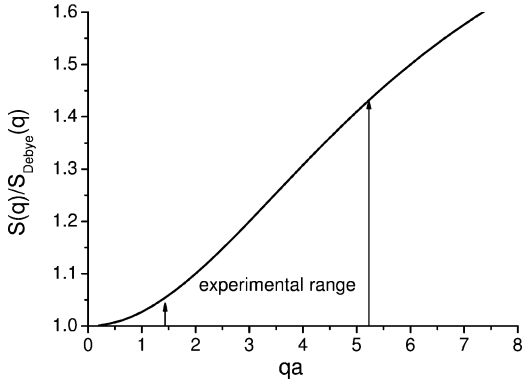

Figure 2. Deviation of static structure factor of the tube theory (eq 2) from the Debye structure factor, eq 3.

not a Debye function for $qa \sim 1$, but significantly larger and expressed by eq 2. Figure 2 shows the ratio of the structure factor of eq 2 to the Debye structure factor for $qR_g \gg 1$. One can see that, in the experimental range deviations reaching 50%, making any comparison quite meaningless.

This contradiction leads one to recognize the rather obvious fact that the model for describing the dynamic structure factor for $qa \sim 1$ must be more detailed than the tube theory (in fact, the original de Gennes paper stated this very clearly). In particular, it must contain a transition to Rouse dynamics for short time scales and obey unperturbed random-walk statistics at all length scales (note that expression 6 does not contain a fast Rouse relaxation for $t < \tau_e$). In the next section, I construct one such possible model.

3. Single-Chain Slip-Links Model

In this section I will develop a dynamic one-chain model of entangled polymers. The original idea of slip-links in the context of polymer networks was proposed in ref 13 and further developed in ref 12. I start from the free Rouse chain in three dimensions (which is a good model for unentangled polymer melts), consisting of $N + 1$ beads (from 0 to N), connected by N springs. The Kuhn segment of the chain is b and the mean-square end-to-end distance is Nb^2. We assume that each bead has a friction coefficient ξ, arising from fast collisions with other chains, but not from entanglements. Now we have to introduce the influence of entanglements, which is believed to be long-lived and topological. The simplest way to introduce it is to argue that the chain monomers experience some mean field, and the simplest possible field is parabolic: $U = \kappa(\mathbf{r}_i - \mathbf{a}_i)^2$, where $\mathbf{r}_i$ is the position of the monomer i, $\mathbf{a}_i$ is the center point of this potential, and κ is the strength of the potential. It is useful to visualize this potential as a set of additional springs, which connect monomers to anchoring points $\mathbf{a}_i$. We can also imagine that these additional springs are pieces of the same polymer, so that the linear chain becomes a comb chain, attached to the solid elastic background by its teeth. The potential then has the form $U = 3k_BT/(2N_sb^2)(\mathbf{r}_i - \mathbf{a}_i)^2$, where N_s is a number of monomers in the additional virtual springs.

The next step is to introduce reptation-like motion by recognizing that the additional springs should not be permanently attached to a particular monomer, but can slide from one monomer to another. This can be visualized as slip-links attached to the anchoring points (see

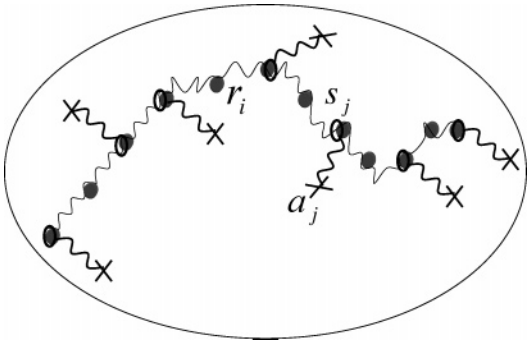

Figure 3. Slip-links model of entangled polymer chain. Spheres connected by the thin springs represent a standard Rouse chain, thick springs are additional potentials, attached to slip-links on a chain $\mathbf{s}_j$ and to fixed anchoring points $\mathbf{a}_j$ (crosses).

Figure 3). Rubinstein and Panyukov considered this case in their recent paper,[10−12] applied to the deformed network. However, they did not address the dynamics of relaxation, and did not consider disentanglement and reentaglement at the ends of the linear chains. These two issues are crucial for the present model.

To introduce tractable dynamics, suitable for computer modeling and analytical solution, I introduce a continuous variable $x = 0...N$ along the chain, and allow each slip-link to be anywhere on the chain, not necessarily at some particular monomer. I argue that the microscopic details should not matter for long-time behavior, and thus, for simplicity, assume that the slip-links travel along the straight lines between neighboring monomers. The total potential energy of the chain is then

$$U = \frac{3k_BT}{2b^2}\sum_{i=0}^{N-1}(\mathbf{r}_{i+1} - \mathbf{r}_i)^2 + \frac{3k_BT}{2N_sb^2}\sum_{j=1}^{Z}(\mathbf{a}_j - \mathbf{s}_j(x_j, \{r\}))^2 \quad (7)$$

where

$$\mathbf{s}_j(x_j,\{r\}) = \mathbf{r}_{\mathrm{trunc}(x_j)} + (x_j - \mathrm{trunc}(x_j))(\mathbf{r}_{\mathrm{trunc}(x_j)+1} - \mathbf{r}_{\mathrm{trunc}(x_j)}) \quad (8)$$

is the position of the slip-link number j, trunc(x) is the closest integer to x less than or equal to x. Here $Z = N/N_e$ is the number of slip-links per chain, N_e is an average number of Kuhn segments between slip-links, i is the monomer index, and j is the slip-link index. The advantage of this particular potential is that we can easily find the distribution of the anchoring points $\mathbf{a}_j$, which will lead to unperturbed Gaussian statistics of the original chain. To do this, I start by generating a free Gaussian chain, then choose positions of slip-links x_j randomly from 0 to N and then generate positions of the anchoring points $\mathbf{a}_j$ distributed around $\mathbf{s}_j$ according to Boltzmann weight $P(x_a) \sim \exp(-3k_BT/(2N_sb^2)(\mathbf{s}_j - \mathbf{a}_j)^2)$. Now, for any dynamics of such a system, which preserves Boltzmann distribution, the chains will obey unperturbed Gaussian statistics. Indeed, the probability distribution of $\mathbf{r}_i$ for a particular $\mathbf{a}_j$ and x_j is

$$P(\{\mathbf{r}_i\}, \{x_j\}, \{\mathbf{a}_j\}) = \frac{1}{\mathcal{N}} \exp\left(-\frac{3k_B T}{2b^2} \sum_{i=0}^{N-1} (\mathbf{r}_{i+1} - \mathbf{r}_i)^2 - \frac{3k_B T}{2N_s b^2} \sum_{j=1}^{Z} (\mathbf{a}_j - \mathbf{s}_j(x_j, \{r\}))^2 \right) \quad (9)$$

We now can average over different realizations of anchoring points $\mathbf{a}_j$ by integrating eq 9 over them. Because of the structure of the potential, the result will not depend on x_j:

$$\int P(\mathbf{r}_j, x_j, \mathbf{a}_j)\, d\mathbf{a}_j = \frac{1}{\mathcal{N}'} \exp\left(-\frac{3k_B T}{2b^2} \sum_{i=0}^{N-1} (\mathbf{r}_{i+1} - \mathbf{r}_i)^2 \right) \quad (10)$$

This proves that the model indeed satisfies unperturbed Gaussian statistics on all length scales and thus produces the correct structure factor, provided the distribution eq 9 is satisfied at all times. We also check chain statistics routinely in simulations by plotting second and fourth moments of the distance between different monomers and comparing them with the theoretical values for the Gaussian chain; the deviations are within 2% and decrease with decreasing the time steps.

The potential eq 7 allows calculation of forces acting on the chain monomers and the slip-links. To formulate a stochastic equation of motion for the slip-links, satisfying Boltzmann distribution for all variables, one also needs to introduce random forces, acting on x_j, and associated friction ξ_s. This leads to the following stochastic equation of motion for the chain and the slip-links position along the chain:

$$\xi \frac{d\mathbf{r}_i}{dt} = \frac{3k_B T}{b^2}(\mathbf{r}_{i+1} - 2\mathbf{r}_i + \mathbf{r}_{i-1}) + \mathbf{f}_i(t) + \frac{3k_B T}{N_s b^2} \sum_{j:\mathrm{trunc}(x_j)=i} (1 - (x_j - \mathrm{trunc}(x_j)))(\mathbf{a}_j - \mathbf{s}_j) + \frac{3k_B T}{N_s b^2} \sum_{j:\ \mathrm{trunc}(x_j)=i-1} (x_j - \mathrm{trunc}(x_j))(\mathbf{a}_j - \mathbf{s}_j) \quad (11)$$

$$\xi_s \frac{dx_j}{dt} = \frac{3k_B T}{N_s b^2}(\mathbf{r}_{\mathrm{trunc}(x_j)+1} - \mathbf{r}_{\mathrm{trunc}(x_j)})(\mathbf{a}_j - \mathbf{s}_j) + g_j(t) \quad (12)$$

Here $\mathbf{f}_i(t)$ and $g_j(t)$ are random forced with zero mean, satisfying the fluctuation−dissipation theorem:

$$\langle f_i(t) f_j(t') \rangle = 2k_B T \xi \mathbf{I} \delta(t - t') \delta_{ij}; \qquad \langle g_i(t) g_j(t') \rangle = 2k_B T \xi_s \delta(t - t') \delta_{ij}$$

where $\mathbf{I}$ is the unit tensor. The set of two equations, 11 and 12, forms a complete description of the one-chain model. The first equation for the chain has two Rouse terms (regular and stochastic) and two additional forces from the slip-links on the right and on the left of the bead $\mathbf{r}_i$. The second equation for the slip-link position x_j has a regular force from the attached spring (projected on the line between two neighboring monomers) and a random force. The regular forces in both equations are easily obtained by differentiating the potential eqs 7, 8 with respect to corresponding coordinate. I also do not allow slip-links to pass through each other, which makes a very small difference in the results but seems to be more natural choice.

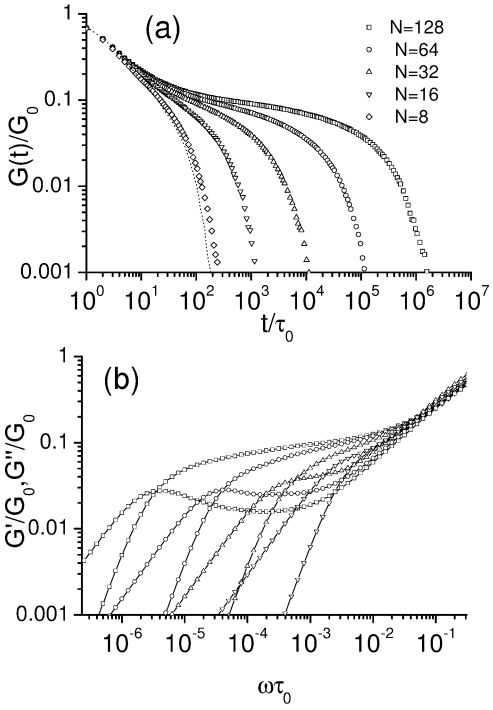

Figure 4. Linear relaxation modulus $G(t)$ (a) and loss and storage modulus (b) for $N = 8$, 16, 32, 64, and 128.

The only missing component is the constraint release, which I introduce by the method used in most recent slip-links simulations.[16,17] I simulate an ensemble of chains, keeping a table of binary correspondences between the slip-links. When one chain gets rid of the slip-link by passing its end through it, this and the corresponding slip-link on the other chain disappear. Then, two new slip-links appear in the system: one at the end of randomly chosen chain, and another in any place of another chain. This completes the description of this rather simple model. The slip-link friction ξ_s is a new unusual parameter in the model, and I shall discuss its origin and optimal choice in the next section.

4. Results

I shall start discussion of the results by presenting model predictions for NSE, rheology, and self-diffusion for one particular set of parameters (N_s, N_e, and ξ_s), which seems to be an optimal choice. After that, I will discuss how this choice of parameters was made. I chose to put slip-links every 4 beads on average, i.e., $N_e = 4$, and set a spring strength to $N_s = 1/2$. Then I choose the friction coefficient of the slip-links ξ_s to be much smaller than the friction of the chain segments ($\xi_s/\xi = 0.1$).

To calculate the linear stress relaxation function $G(t)$, I calculate the off-diagonal stress−stress correlation function, which is equal to $G(t)$ by the fluctuation−dissipation theorem. Note that Rubinstein and Panyukov[12] proved that N_s must change with deformation $N_s \sim N_s^{(0)}\sqrt{\lambda}$. However, this effect is only important for nonlinear deformations. Indeed, for small deformations, $\lambda = 1 + \epsilon$, the stress will be $\sigma = \epsilon G_N^{(0)}(N_s^{(0)}\sqrt{1+\epsilon})$. Assuming that $G_N^{(0)}(N_s)$ is a smooth function of N_s, we get $G = \lim_{\epsilon \to 0} \sigma/\epsilon = G_N^{(0)}(N_s^{(0)})$.

Figure 4a shows stress relaxation for different chain lengths ($N = 8...128$). Stress here is given in units of

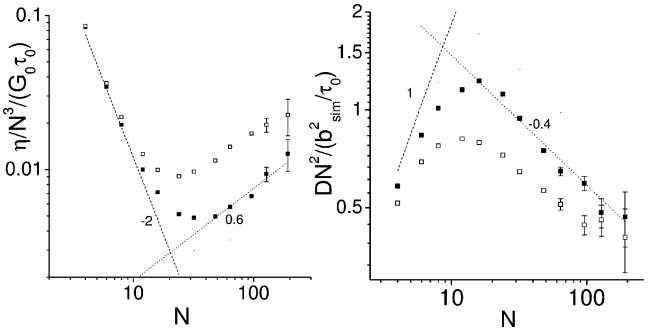

Figure 5. Normalized viscosity (a) and self-diffusion coefficient (b) predictions with and without constraint release (filled and open symbols correspondingly). Rouse model predictions are shown by dotted lines, −0.4 and 0.6 slopes by dashed lines.

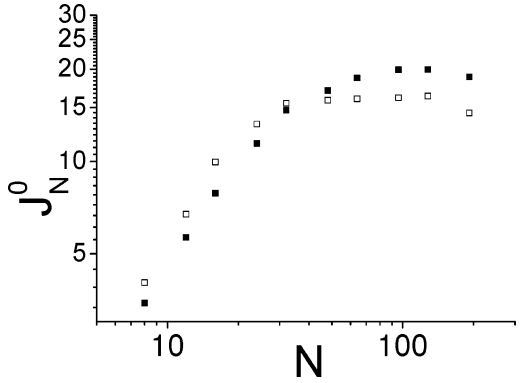

Figure 6. Zero shear-rate compliance as a function of chain length with and without constraint release (filled and open symbols correspondingly).

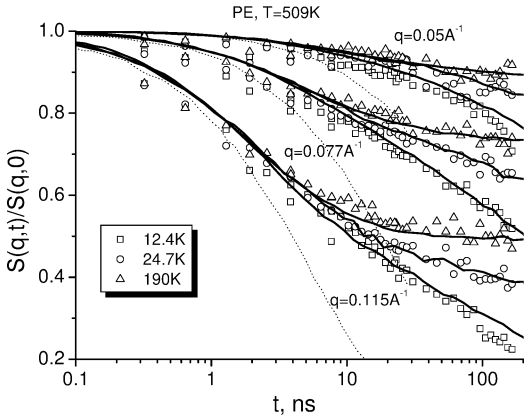

Figure 7. Comparison of normalized dynamic structure factor predicted by the model and measured by NSE for three different molecular weights of PEB-2 at three different q-vectors (see legend).

$G_0 \equiv \rho RT/M_0$, where M_0 is molecular weight represented by one bead. This is a natural simulation unit of stress and should not be confused with the plateau modulus $G_N^{(0)}$. One can see that at $N = 8$ (not shown in Figure 4b for clarity) stress relaxation is almost Rouse-like (dotted line), and then the characteristic plateau develops with increasing N. By fitting $G(t)$ with a spectrum of equidistant Maxwell modes, we transform it to the complex modulus, G' and G'', which are shown in Figure 4b. The shape of G' and G'' looks consistent with experimental observations; for example the intermediate slope of G'' approaches to $-1/4$ for large N.

Figure 5 shows viscosity and self-diffusion coefficient predictions as a function of chain length N. Note that I will use reduced quantities η/N^3 and DN^2 in all comparisons below. This has several advantages: it greatly reduces the scale of the vertical axis, and the transition between slopes 0.4−0.6 and 0 in experimental data becomes clearly visible. Naturally, viscosity is also normalized by $G_0\tau_0$ and the diffusion coefficient by $b_{\mathrm{sim}}^2/\tau_0$, where $Nb_{\mathrm{sim}}^2 = \langle R^2 \rangle$ is the end-to-end distance of the chain, and b_{sim} is a Kuhn segment of the chain in simulations.

Note several features of these plots. For small N, both the viscosity and diffusion coefficients follow Rouse model predictions. Than, there is a rather sharp transition to approximately $\eta \sim N^{3.6}$ behavior, with crossover around $N_c = 16$ (with CR). This is slightly different from our earlier analytical model,[19] which goes through higher slope around 3.8−3.9 before smooth transition to slope 3. Similarly, the diffusion coefficient shows −2.4 slope (−0.4 on this graph). Unfortunately, it is not yet possible to determine where this model predicts transition to pure reptation behavior, which would correspond to horizontal lines in both plots. Diffusion predictions without constraint release (open symbols in Figure 5b) correspond to diffusion of linear chain in a network or in a matrix of much longer chains. The error bars on last 2 points are quite big, which prevents me from making the definite conclusion that transition to zero slope is predicted.

Figure 6 shows predictions for zero shear-rate compliance $J_N^{(0)}$. Again, contrary to our early predictions, there is no pronounced maximum in this plot, and the Rouse regime $J_N^{(0)} = 2/5\, N$ smoothly goes to the plateau, predicted by reptation.

Figure 7 compares prediction of the model for dynamic structure factors with NSE data on monodisperse polyethylene (PEB-2).[14] To fit all three molecular weights simultaneously, we used ($\xi_s/\xi = 0.01$), whereas ($\xi_s/\xi = 0.1$) were used for all other plots. This is a little unsatisfactory and introduces about 30% difference in viscosity and diffusion data. However, it makes it consistent with our follow-up paper,[21] where we show that this choice of parameters allows fitting of NSE data for a variety of binary bleeds. It is evident that the agreement in Figure 7 is good, and the model fits all q-vectors and all molecular weights with the same parameters. The square roots of mean-square distance between experimental points and simulations are 0.025, 0.021, and 0.017 for 12, 25, and 190 K molecular weights, respectively. This can be compared with fits by modified tube theory from ref 14, which give 0.0221, 0.0191, and 0.0197, respectively. Clearly, the quality of fits is very similar. Good agreement is also achieved for binary mixtures of different molecular weights.[21] Here I used $\tau_0 = 0.07$ ns as a fitting parameter. More details on the fitting procedure of the NSE data is given in the next section.

Now we can discuss how the model parameters affect predictions described above. Unlike the tube theory, the slip-links model seems to have three entanglement-related parameters (N_s, N_e, and ξ_s) instead of a single N_e of the tube theory. However, only the combination of the first two defines a plateau modulus[12] and terminal properties, whereas their particular values have very little effect, mainly on the shape of transition between the Rouse and the plateau region. This is a nontrivial numerical result. To illustrate this point, I set $N_e = 1$, 2, and 4 for $N = 64$ and adjusted N_s so that the plateau modulus is the same (correspondingly N_s values were

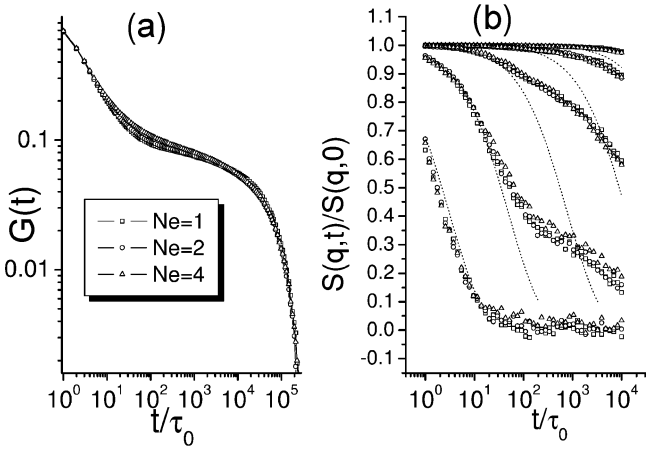

Figure 8. Rheology (a) and NSE (b) predictions for different sets of N_s/N_e.

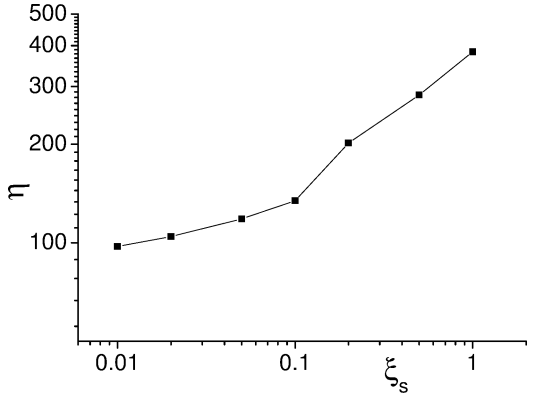

Figure 9. Viscosity of the chain $N = 32$ as a function of slip-link friction.

$N_s = 4$, 1.75, and 0.5). Figure 8 shows that $G(t)$ and $S(q, t)$ for $qb_{sim} = 0.25$, 0.5, 1, 2, 4 are almost indistinguishable.

The third parameter ξ_s is an additional artificial friction of slip-links along the chain. As we do not want any physical parameters to depend strongly on it, we chose $\xi_s \ll \xi_0$. In this limit, dependence on ξ_s is logarithmic and may be ignored in most cases. Note that it is not possible to set $\xi_s = 0$, as this will result in zero escape time of the slip-link from the chain. On the contrary, for nonzero ξ_s, this escape time is exponentially dependent on the potential of virtual springs and only linearly on ξ_s. Figure 9 demonstrates that viscosity for $N = 32$ changes with ξ_s slowly for $\xi_s \leq 0.1$, in particular, between $\xi_s = 0.1$ and 0.01, it drops only 30% for factor of 10 change in ξ_s.

Now I will briefly make a connection with our previous analytical solution for the "standard" tube model.[19] Figure 10shows comparison of the linear rheology predicted by the single-chain slip-link model with and without constraint release with our previous analytical model.[19] The fitting parameters for the analytical model are

$$G_e = 0.134G_0, \quad \tau_e = 79\tau_0, \quad \text{and } M_e = 7 \quad (13)$$

Looking at the left graph, one can conclude that if both models do not have constraint release, the agreement is satisfactory even for $N = 48$, which corresponds to about $Z = 7$ entanglements in analytical model. When one adds constraint release, there is an additional choice of constraint release parameter in the analytical model

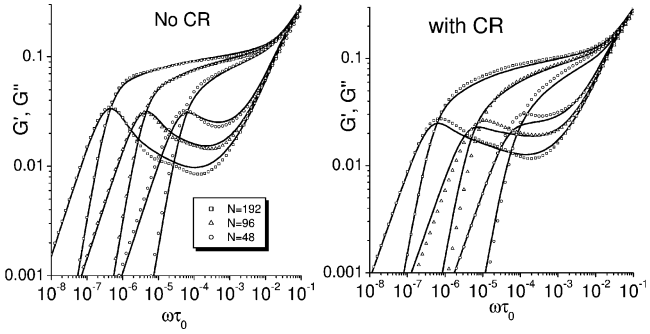

Figure 10. Linear rheology predictions of the slip-links model (symbols) compared with the "standard" tube model from ref 19 (lines). Left graph is comparison without constraint release in both models, right graph, with constraint release included in both models.

c_v (see ref 19 for details). It appears that $c_v = 0.1$ is the best choice to fit data for the longest chains (see Figure 10), but agreement gets worse as the chain length decreases. The constraint release algorithm used in the slip-links model is different from the Rubinstein−Colby algorithm used in ref 19, thus the difference in predictions is not surprising. The Rubinstein−Colby model assumes that the mobility of the tube segment due to the entanglement constraint is fixed to the particular tube segment, whereas in the slip-link model (and probably in reality) the constraint diffuses along the chain, thus speeding up the disentanglement process.[17]

Our previous finding that $c_v = 0.1$ fits experimental data slightly worse than $c_v = 1$ is probably connected with polydispersity. Indeed, I found that polydispersity $PI = 1.03$ is enough to change the shape of G'' from $c_v = 0.1$ to $c_v = 1$.

Note again that the standard tube model does not allow prediction of the dynamic structure factor using the same assumptions as used in rheology theory. It is also usually assumed that the number of entanglements is sufficiently large, thus the transition from unentangled to entangled dynamics cannot be accurately described. Thus, we now proceed to direct comparison of the single-chain slip-links model with experiments for five different polymers.

5. Parameter Mapping and Comparison with Experiment

In this section, I will make an attempt to compare model predictions simultaneously with several experimental techniques (NSE, rheology, and self-diffusion) using the same parameters for chemically identical samples. Note that this is very rarely done in the literature, and usually, one does not expect perfect agreement (even the same experiments done in different groups sometimes differ significantly). An additional complication is uncertainty in the time−temperature superposition procedure, which is needed because the three techniques use quite different temperatures. Nevertheless, I will show that potentially much can be learned from such systematic comparison and will try to stimulate more work in this direction. Table 1. summarizes all parameters used in the fitting, where the first three columns give time−temperature superposition parameters according to $\log_{10}(a_t) = -C_1(T - T_0)/(T + C_2)$ and the fourth chain dimension expansion coefficient $\kappa = d \ln(\langle R^2 \rangle)/dT$. The next two columns contain elementary times extracted from NSE and linear rheology correspondingly. Then, b_{sim} value is

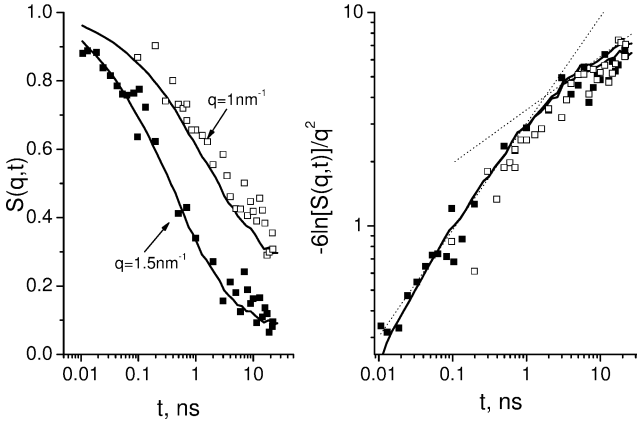

Figure 11. Incoherent dynamic structure factor of long polyethylene chains at $T = 509$ K from (ref 15) compared with the model predictions.

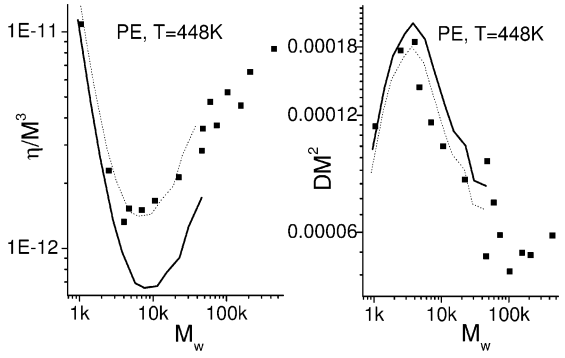

Figure 12. Normalized viscosity and diffusion coefficient compared with the data of ref 18. Solid lines: predictions using parameters from NSE; dotted lines: best fits using M_0 as fitting parameter.

obtained from either fitting of NSE data or linear rheology, elementary stress G_0 from fitting the linear rheology data. The last three columns are values of M_0, which is roughly proportional to M_e of the tube model (see eq 13), extracted from NSE, from the form of G'/G'' spectra and from the value of the plateau modulus.

5.1. Polyethylene (PE). Monodisperse polyethylene is available as hydrogenated polybutadiene and is often referred to as PEB-2. It is the only polymer that is extensively studied by NSE for times well over τ_e and for a variety of molecular weights (see ref 14 and references therein). Thus, I will fit the model to NSE experiments first and then predict rheology and diffusion. As already discussed, this fitting is done in Figure 7, giving model parameters $b_{sim} = 15.3$ Å, $\tau_0(T = 509\text{ K}) = 0.07$ ns. Here, b_{sim} is the unit length of the model, and it is proportional to the "tube diameter" because we have the same number of beads between entanglements for all polymers. Knowing the mean-square end-to-end distance per unit mass from ref 20, $K \equiv \langle R^2\rangle/M = 1.08A^2$ mol /g, we determine the unit mass, represented by one bead $M_0 = b_{sim}^2/K = 216$ g/mol. We thus used 57 and 116 beads to simulate 12.4 and 24.7 K polyethylene in Figure 7.

Figure 11 shows comparison of the model predictions for the incoherent structure factor measured in ref 15 for the same high M_w sample as in Figure 7 at the same temperature $T = 509$ K. I give this comparison in two representations, one is actual measured data and another represents the mean-square monomer displacement for some models (this is shown not to be strictly valid for the tube model in ref 27). One concludes that the agreement is satisfactory, and in some sense, the incoherent structure factor provides information about entanglements similar to that of the coherent one.

Now we predict plateau modulus, viscosity, and diffusion coefficients to compare them to the data by Pearson et al.[18] All stresses calculated in simulations must be multiplied by $G_0 = \rho RT/M_0$, viscosities by $G_0\tau_0$, and diffusion coefficients by b_{sim}^2/τ_0. The data in ref 18 are given for $T = 448$ K, and we calculate $\tau_0(T = 448\text{ K}) = 0.14$ ns using shift factors given in the same paper. Calculating all prefactors mentioned above, we arrive at Figure 12, denoted by solid lines. The dotted lines are best fits of the data using M_0 as a fitting parameter. One can see that diffusion data are predicted rather well (dotted line correspond to $M_0 = 206$ g/mol, to be compared with 216 g/mol from NSE), but viscosity data is significantly off and requires a large adjustment of $M_0 = 180$ g/mol. With our choice of model parameters, the plateau modulus (defined as 3.56 times maximum value of G'' for long chains) is about $G_N^{(0)} = 0.1G_0$. Thus, for polyethylene, we predict the plateau modulus to be about 1.3 MPa, but the experimental value is about 2.2 MPa. We conclude that, for polyethylene, diffusion may be well predicted by knowing the dynamic structure factor, but rheology predictions requires smaller M_0 or equivalently more entanglements. This conclusion is similar to the conclusion of ref 7, where authors showed that the plateau modulus of polyethylene gives smaller M_e values than any other definitions. Each separate experiment, however, can be well fitted by the model, including the slope and the shape of viscosity and diffusion curves. Unfortunately, it was computationally prohibitive to run the model for higher chain lengths to establish whether a transition to horizontal lines in Figure 12 is captured.

5.2. Polyethylene-propylene (PEP). This is another polymer for which existing NSE data[15] allows fixing of all model parameters, although only high molecular weight is measured. Figure 13 shows the best fit of the data using two parameters: $\tau_0(T = 492\text{ K}) = 0.39$ ns, $b_{sim} = 19$ Å. The quality of fit, defined in the previous section, is 0.0257, compared with the 0.0329 fit by the tube theory expression.

One great advantage of PEP as compared to PE is that PEP does not crystallize at low temperatures, and thus whole G′/G″ curves can be measured and compared to the model. Figure 14 shows rheology data shifted to reference temperature 298 K for the same sample ($M_w = 243$ K), as was used in ref 15, compared with the model predictions using parameters obtained by NSE (thick lines). One should pay attention only to the high-

Table 1. Parameters for Mapping Slip-Links Model to Different Experimental Techniques

	C_1	C_2 (°C)	T_0 (°C)	$10^3\kappa$	τ_0^{nse} $(T)(ns)$	τ_0^{rheo} $(T)(ns)$	b_{sim} (Å)	G_0 (MPa)	M_0^{NSE}	M_0^Z	M_0^G
PE				−1.1	0.07 (509)	–	15.3	21	216	–	130
PEP	6.27	132	25	−1.1	0.35 (492)	0.02 (492)	19	11	480	214	246
PI	4.8	113	25	0.4		130−400 (298)	18	4.3		590, 770	520
PBd	3.52	139	25	≈ 0	2.6 (298)	4.5 (298)	14.8	11.2		250	193
PS	5.53	−52	170	≈ 0	2800 (453)	29.4	2.2			2000	1600

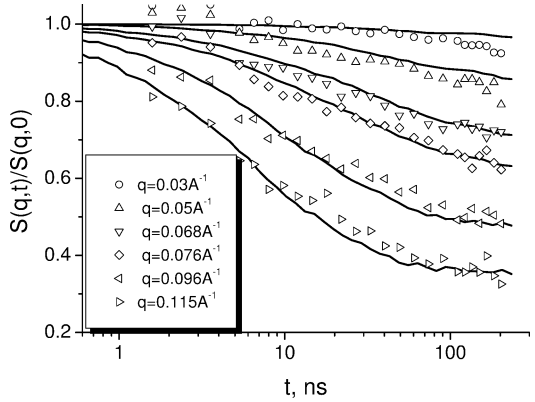

Figure 13. Normalized dynamic structure factor as measured by NSE from ref 15. Solid lines: best fits by the model.

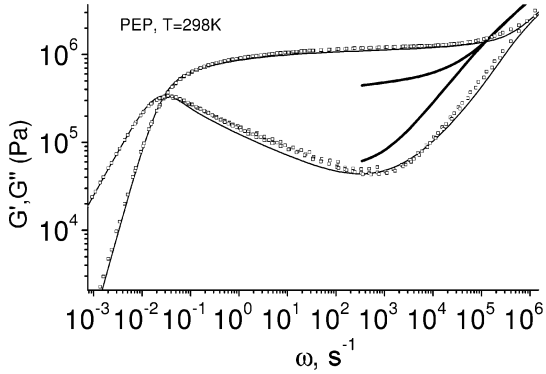

Figure 14. Linear rheology of the same PEP sample as used in ref 15. Solid lines: predictions with parameters obtained from NSE; dotted lines: best fits by the model. Only the high-frequency region can be compared.

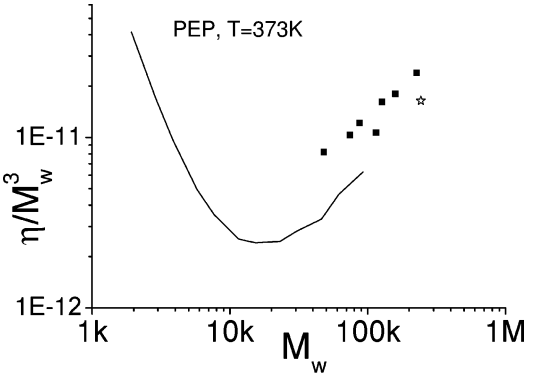

Figure 15. Normalized viscosity data from ref 23 (star is viscosity of sample from Figure 14) compared to the model predictions with parameters obtained from NSE.

frequency region, as it was not possible to simulate such large chains (thus the terminal region is not shown). The high-frequency region shows that the predictions are totally wrong; τ_0 is off by a factor of 16, and the plateau value by a factor of 2.5 (see Table 1). Thin lines show best fit of the data with our analytical model.[19] One concludes that the model fails to describe NSE and rheology of PEP simultaneously, similarly to PE.

Figure 15 shows the only existing data on viscosity of PEP as a function of molecular weight.[23] Unfortunately, the narrow range of molecular weights does not allow determination of M_0 from these data, but strangely, enough existing data are in relatively good agreement with the model predictions, maybe because the temperature used was quite high.

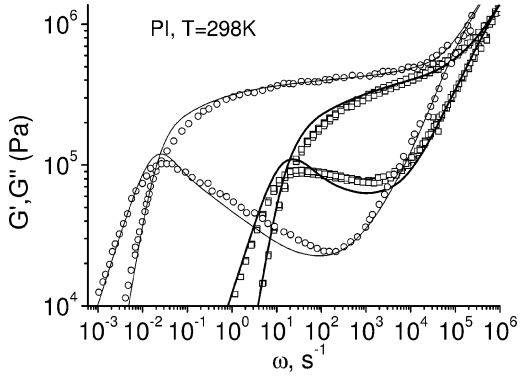

Figure 16. Linear rheology data for polyisoprene of M_w = 75 K from ref 24 (squares) and of M_w = 500 K from ref 25 (circles). Squares are fitted by slip-links model, and circles, by analytical model.

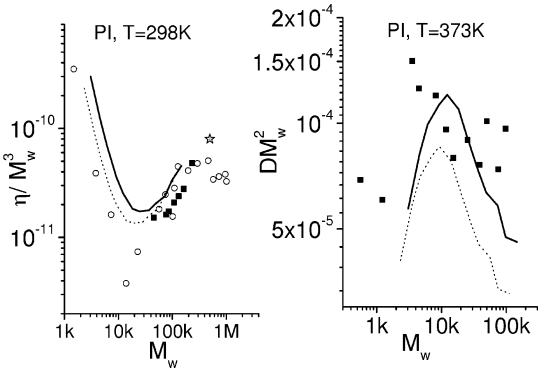

Figure 17. Normalized viscosity and self-diffusion data for polyisoprene as a function of molecular weight. Viscosities are from ref 23 (squares), ref 24 (circles), and ref 25 (star); diffusion from ref 22. Solid lines are predictions by the model using linear rheology from ref 25, dotted lines from ref 24.

5.3. Polyisoprene (PI). As no long-time NSE data is published for polyisoprene at the moment, we use linear rheology to fit the model parameters. However, the rheology data in the literature are quite contradictory, especially at high frequency/low temperature. Figure 16 shows the data from ref 24 for polyisoprene of M_w = 75 K compared to older data for M_w = 500 K from ref 25. The first dataset is fitted by the model with G_0 = 4 MPa, $\tau_0(T$ = 298 K) = 180 ns, and M_0 = 586 g/mol, and the second by an analytical model using eq 13 (because the number of entanglements is too high to be simulated by slip-links). By using mapping of an analytical model to the slip-links model eq 13, I get G_0 = 4 MPa, $\tau_0(T$ = 298 K) = 400 ns, and M_0 = 767 g/mol. One can see that the difference in τ_0 is significant, which is clearly visible in the high-frequency part of Figure 16.

We now use obtained parameters from both datasets of Figure 16 to predict viscosity and diffusion coefficients reported in refs 22, 23, 24, as shown in Figure 17. Both viscosity and diffusion are captured rather well, taking into account the large scatter. More measurements on polyisoprene are highly desirable.

5.4. Polybutadiene (PBd). Unfortunately, NSE data for polybutadiene is available only for short times and unentangled samples.[29] Also, very little diffusion data is available. Besides, the rheology data is published for well-entangled samples M_w > 50 K, which are difficult to simulate at the moment. Thus, I fit parameters to one dataset[31] for M_w = 48 K at reference temperature T = 25 °C, which is shown in Figure 18. The fitting

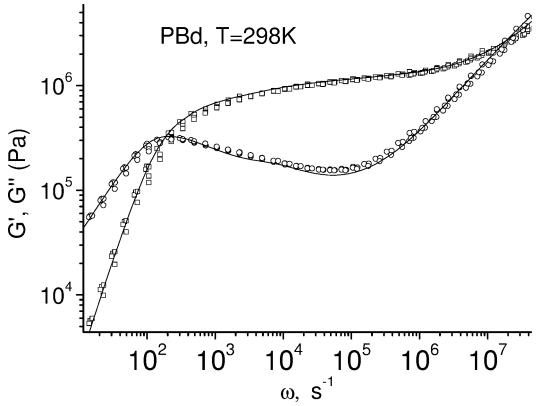

Figure 18. Storage and loss moduli of polybutadiene with $M_w = 48$ K, measured in ref 31, compared with the slip-links model (solid lines).

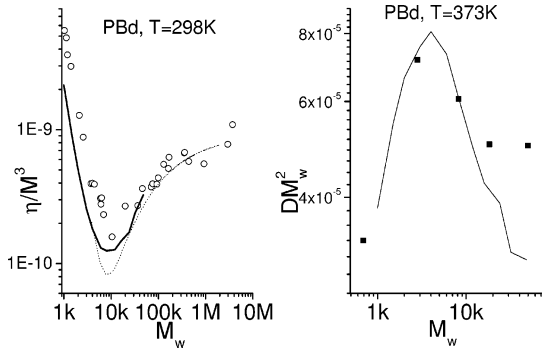

Figure 19. Normalized viscosity and self-diffusion data for polybutadiene as a function of molecular weight. Viscosities are from ref 28, diffusion from ref 22. Solid lines are predictions by the model, with parameters obtained from the fit of linear rheology data; dotted line: predictions of our earlier analytical theory.[19]

parameters are $\tau_0 = 3.5$ ns, $G_0 = 12$ MPa, and $M_0 = 250$ g/mol. The M_0 value leads to prediction of $G_0 = 9$ MPa, smaller than the fitted value by 30%, which is 2 or 3 times bigger than the typical experimental error.

Using the obtained parameters, we make predictions for viscosity and diffusion and compare them with data from refs 28 and 22 correspondingly, as seen in Figure 19. The agreement is quite satisfactory, but more diffusion data is highly desirable. One can also compare an elementary time scale τ_0 to unentangled NSE data from ref 29 for $M_w = 1.6$ K. Fitting the Rouse model to three datasets with the lowest q (at higher q, Rouse theory breaks down as discussed in ref 29), I get $\tau_0 = 0.3$ ns at $T = 353$ K. Taking into account glass transition temperature dependence on molecular weight for small molecular weights, I get an estimate $\tau_0(298\text{ K}) \approx 2.6$ ns, which is 80% different from rheology estimate (see Table 1). This difference is, however, nowhere near the dramatic difference of PEP time scales.

5.5. Polystyrene (PS). Polystyrene has a significantly larger molecular weight between entanglements than compared to that of the previous polymers, and the linear rheology data for mildly entangled polymers is available.[30] In Figure 20, we plot G' and G'' from ref 30 of $M_w = 34$, 61, and 125 K, measured at $T = 180$ °C and the model predictions using fitting parameters $\tau_0 = 2800$ ns, $G_0 = 2.2$ MPa, and $M_0 = 2$ K. First, note that these fits are good, given that previous theories failed to describe polymers with such few entanglements. Also, the value of G_0 is consistent with M_0; indeed, using $\rho = 959 kg/m^3$, we get $G_0 = \rho RT/M_0 = 1.8$ MPa, which is within typical differences between the data in different papers.

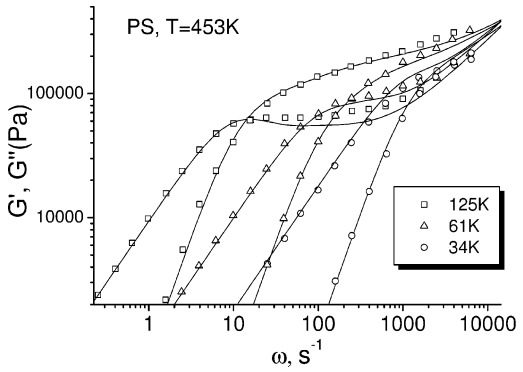

Figure 20. Storage and loss moduli of polystyrene with $M_w = 34$ K, 61 K, and 125 K, measured in ref 30, compared with the model (solid lines).

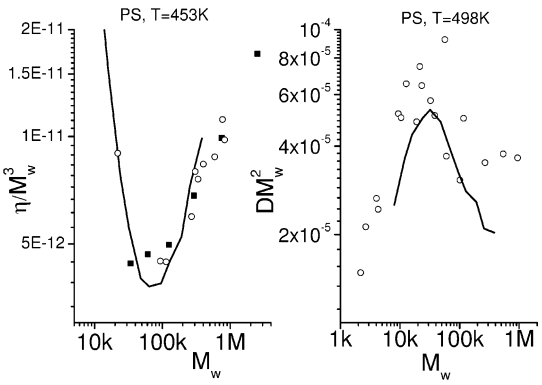

Figure 21. Normalized viscosity and self-diffusion data for polystyrene as a function of molecular weight. Viscosities are from ref 30 and ref 4, diffusion from ref 4. Solid lines are predictions by the model, with parameters obtained from the fits in Figure 20.

In Figure 21 we plot viscosity data for all six samples reported in ref 30, together with viscosity and diffusion data on polystyrene collected by Watanabe[4] from different sources. The agreement for polystyrene seems to be quite satisfactory, although experimental viscosity data seem to have slightly smaller slopes than that of the model predictions.

6. Conclusions

To conclude, in this paper I stressed the distinction between a model and the theory, describing a particular model. I demonstrated that the standard tube model (one-dimensional Rouse chain in three-dimensional random walk tube) is not complete and cannot be directly compared to the dynamic structure factor measured by NSE. Instead, for each experiment, different interpretations ("theories") of the tube model were used. For example, for linear rheology, fast 3D Rouse modes were added rather empirically, whereas they were ignored in the NSE comparison. But an even more important problem of the standard tube model is its failure to describe the static structure factor at the length scale of order of the tube diameter. In other words, the tube model violates random walk statistics, a fact that is not easy to fix empirically.

These considerations led to the development of the new single-chain slip-links model, on the basis of

Rubinstein's and Panyukov's model for polymer networks.[12] The main difference of this model from the tube model is that an effective field, representing entanglements, is introduced in a discrete fashion as a set of additional parabolic potentials (slip-links). In this way, it is possible to construct this field so that the chain exactly satisfies random walk statistics at all length scales. The model automatically contains reptation, contour length fluctuations, fast Rouse, and longitudinal modes, and constraint release is added in the usual manner.

Acknowledgment of the difference between the theory and the model suggests the importance of direct comparison between the model and experiment, which would avoid approximations involved in an analytical solution of the model. Thus, in this paper, I performed Brownian dynamics simulation of the constructed model and compared it with NSE, rheology, and diffusion experiments. Because the nature of all slip-links models, the new model has three new parameters instead of one of the usual tube model. However, I showed that the number of slip-links and their strength enter the results only in combination, and that dependence on slip-link friction is insignificant, providing it is much smaller than the monomer friction. The detailed role of these parameters needs further investigation.

I demonstrated that each separate experiment can be well described, but also attempted the more challenging task of obtaining all fitting parameters from one experiment and predicting all other with the same parameters.

This procedure was quite successful for polybutadiene, polystyrene, and polyisoprene, although no NSE data is available yet for these polymers. The data for polyisoprene[22] are contradictory at the moment, and more experiments are needed to clarify the situation with PI parameters. For polyethylene and polyethylene-propylene, however, it seems that fitting rheology requires a smaller M_0 (roughly proportional to M_e in the tube model), compared to that of NSE and diffusion. This probably suggests that these polymers cannot be described by the Rouse model at small time and length scales. Indeed, the validity of the Rouse model was demonstrated for short PE chains to hold only for large enough q in NSE experiments and break down for $q > 0.15nm^{-1}$. In linear rheology, the Rouse model predicts parallel G′ and G″, which is never observed for any polymer melt. Thus, at the moment, one cannot be sure about the area of applicability (if any) of the Rouse model. The dependence of these discrepancies on packing length is an intresting subject for further investigation, which requires more accurate diffusion, rheology, and NSE data.

Another possible reason for strong disagreement of time scales in PEP data is the change of chain dimensions with temperature. I note that the temperature expansion coefficient $\kappa = d\ \ln(\langle R^2\rangle)/dT$ is very different for the polymers under consideration (see Table 1). Nonzero κ makes time−temperature superposition not strictly valid (because tube diameter or M_0 will also change), and the low-temperature estimate of τ_0 may be so much different from NSE results.

One should note a smaller but noticeable discrepancy, which concerns linear rheology only. Last two columns of Table 1 suggest that for PI, PBd, and PS, M_0 (or M_e) obtained from a plateau modulus is lower than the one obtained from fitting G'/G''. This was also noticed in ref 33 for atactic and head-to-head polypropylene.

Acknowledgment. This work was supported by an EPSRC Advanced Research Fellowship. I acknowledge very useful discussions with Michael Rubinstein and Ralf Everaers at the Kavli Institute for Theoretical Physics in Santa Barbara with partial support from the National Science Foundation under Grant No. PHY99-07949, and I thank all members of Forschungszentrum Jülich for stimulating collaboration and providing me with original data. Special thanks to Tom Mcleish for continuous support and interest in my work.

Appendix A. Structure Factor of 1D-Stretched Rouse Chain.

In this appendix, I repeat de Gennes's calculations of the dynamic structure factor for a one-dimensional stretched Rouse chain,[32] but avoiding the approximation made in this paper. The result will then be applied in Appendix B to the chain in a tube. We consider a Rouse chain of N segments of Kuhn length b with friction ξ, which is stretched by the ends so the average length of Kuhn segment is l. In terms of a chain in a tube $l = a/N_e = b/\sqrt{N_e}$, i.e., $l \ll b$.

The coherent structure factor is

$$S^{1d}(q, t) = \sum_{m,n} \langle \exp(iq(r_n(t) - r_m(0))\rangle$$

where summation is over all monomers of one molecule. Neglecting end effects, the sum can be rewritten as

$$S(q, t) = \sum_{n,s} e^{iqls} \langle \exp(iq(y_{n+s}(t) - y_n(0))\rangle$$

where $y_n = r_n - \ln$ is the deviation from the mean monomer position. The average in brackets now can be rewritten using a Gaussian approximation

$$S^{1d}(q, t) = \sum_{n,s} e^{iqls} \exp\left(-\frac{q^2}{2}\langle (y_{n+s}(t) - y_n(0))^2\rangle\right) = \sum_{n,s} e^{iqls} \exp\left(-\frac{q^2\phi_{ns}(t)}{2}\right)$$

where I introduced notation

$$\phi_{ns}(t) = \langle (y_{n+s}(t) - y_n(0))^2\rangle$$

To calculate $\phi_{ns}(t)$, I use transformation to Rouse modes

$$y_n(t) = X_0(t) + 2\sum_{p=1}^{\infty} X_p \cos\left(\frac{\pi ps}{N}\right)$$

and the known correlation functions for X_p (see the Doi−Edwards book,[2] eqs 4.23−4.26). Substituting them into the equation for $\phi_{ns}(t)$ we get

$$\phi_{ns}(t) = \frac{2k_BTt}{N\xi} + \sum_{p=1}^{\infty} \frac{2Nb^2}{3\pi^2p^2} \times \left(\cos^2\left(\frac{\pi p(n+s)}{N}\right) + \cos^2\left(\frac{\pi pn}{N}\right) - 2\cos\left(\frac{\pi pn}{N}\right)\cos\left(\frac{\pi p(n+s)}{N}\right)\exp\left(-\frac{p^2t}{\tau_R}\right)\right) \quad (14)$$

For long chains $N \gg 1$ and $t \ll \tau_R$, the result must be independent of n. One can check numerically that it approximates perfectly with

$$\phi_{ns}(t) = \frac{2k_BTt}{N\xi} + \sum_{p=1}^{\infty} \frac{2Nb^2}{3\pi^2p^2}\left(1 - \cos\left(\frac{\pi ps}{N}\right)\exp\left(-\frac{p^2t}{N^2\tau_0}\right)\right)$$

As expected, for $s = 0$, we recover eq 6.103 from the Doi−Edwards book,[2] and for $t \to \infty$, we get correct asymptotic $2k_BTt/N$. For $t < \tau_R$, we can also neglect the center of mass diffusion the term $2k_BTt/N\xi$ and replace summation by integration because the major contribution to the sum will come from $p \gg 1$:

$$\phi_{ns}(t) \approx \frac{2b^2s}{3\pi^2}h\left(\frac{t}{\tau_0 s^2}\right) \quad (15)$$

where

$$h(R) = \int_0^\infty \frac{dy}{y^2}(1 - \cos(\pi y)\exp(-Ry^2)) = \begin{cases} \frac{\pi^2}{2}, & R \to 0 \\ \sqrt{\pi R}, & R \to \infty \end{cases} (>)$$

The structure factor is then

$$S^{1d}(q,t) = \sum_{n,s}\exp\left(iqls - \frac{q^2 2b^2 s}{2\ 3\pi^2}h\left(\frac{t}{\tau_0 s^2}\right)\right) \approx 2N\int_0^\infty \exp\left(iqls - \frac{q^2b^2s}{3\pi^2}h\left(\frac{t}{\tau_0 s^2}\right)\right)ds \quad (16)$$

We first calculate its values at $t = 0$:

$$S(q,0) = 2N\int_0^\infty \exp\left(\frac{iqbs}{\sqrt{N_e}} - \frac{q^2b^2s}{6}\right)ds = 2N\frac{q^2b^2/6}{q^4b^4/36 + q^2b^2/N_e} = \frac{NN_e}{3}\frac{1}{\frac{q^2a^2}{36}+1} \quad (17)$$

The de Gennes answer was $NN_e/3$, which is the same for $qa \ll 1$, but differs significantly in experimental range of $qa = 1...5$.

The time dependence was evaluated numerically using eq 15 and is perfectly described by single exponential given by de Gennes:

$$S^{1d}(q,t) = \frac{NN_e}{3}\frac{1}{\frac{q^2a^2}{36}+1}\exp\left(-\frac{q^2a^2t}{\pi^2\tau_e}\right) \quad (18)$$

which is the final result for the problem considered. The conclusion of this Appendix is that de Gennes calculations for the scattering function of 1D stretched Rouse chains are confirmed, but for $qa \sim 1$ must be divided by $1 + q^2a^2/36$.

Appendix B. Structure Factor for the Rouse Chain in a Tube.

I now follow de Gennes's 1981 article[3] and implement result eq 18 into the standard tube model. The aim is to calculate the structure factor of a Rouse chain in a tube, which is

$$S(q,t) = \sum_{m,n}\langle[\exp(i\mathbf{q}(\mathbf{r}_n(t) - \mathbf{r}_m(0)))]_{\text{tube}}\rangle_{\text{monomers}} \quad (19)$$

where averages are taken over tube segments orientation $\mathbf{r}(s)$ and over monomer position in the tube $n(s)$. Here s is a contour variable along the tube. Equation 19 can be rewritten as

$$S(q,t) = \int_0^L ds\int_0^L ds'\Sigma(s-s',t)[\exp(i\mathbf{q}(\mathbf{r}(s,t) - \mathbf{r}(s',0)))]_{\text{tube}} \quad (20)$$

where I have defined the 1D density correlation function

$$\Sigma(s-s',t) \equiv \left\langle \frac{di(s,t)}{ds}\frac{di(s'0)}{ds'}\right\rangle_{\text{monomers}}$$

and decoupled the two types of averages. Here $i(s,t)$ is the index number of the monomer that resides in the tube segment s at time t. One can easily see that Σ is related to the structure factor of the 1D stretched Rouse chain, calculated in Appendix A. Indeed

$$S^{1d}(q,t) = \int_0^N dm\int_0^N dn\langle\exp(iq(s(m,t) - s(n,0)))\rangle = \int_0^L ds\int_0^L ds'\Sigma(s-s',t)\exp(iq(s-s')) = L\Sigma(q,t)$$

This means that, to calculate $\Sigma(s,t)$, one needs to calculate the inverse Fourier transform of eq 18:

$$\Sigma(s,t) = \frac{N_e}{b^2} + \frac{N_e^{3/2}}{6\sqrt{\pi}b(1+q^2a^2/36)}\sqrt{\frac{\pi^2\tau_e}{ta^2}}\exp\left(-\frac{s^2\pi^2\tau_e}{4a^2t}\right) \quad (21)$$

where the first constant term is the equilibrium density $\Sigma(s, t \to \infty)$. The second average in eq 20 can be replaced by its Gaussian approximation:

$$[\exp(i\mathbf{q}(\mathbf{r}(s,t) - \mathbf{r}(s',0)))]_{\text{tube}} = \exp\left(-\frac{[(\mathbf{q}(\mathbf{r}(s,t) - \mathbf{r}(s',0))^2)]}{2}\right) = \exp\left(\frac{-q^2a}{6}|s-s'|\right) \quad (22)$$

This approximation contains the postulate that $[(r(s) - r(0))^2] = sa$ on all length scales, even if $s < a$, which causes random-walk statistics violation. Avoiding this assumption is not easy and requires introduction of additional parameters into the model.

Substituting results of eqs 21, 22 to eq 20, we get

$$S(q,t) = \frac{12N}{q^2b^2} + \frac{NN_e}{3(1+q^2a^2/36)}\text{erfc}(\sqrt{t/\hat{\tau}})\exp(t/\hat{\tau}) \quad (23)$$

where

$$\hat{\tau} = \frac{36\pi^2\tau_0}{q^4b^4}$$

and τ_0 is the Rouse time of one Kuhn segment (elementary time scale).

References and Notes

(1) de Gennes, P. G. *J. Chem. Phys.* **1971**, *55*, 572.
(2) Doi, M.; Edwards, S. F. *The Theory of Polymer Dynamics*; Clarendon: Oxford, 1986.
(3) de Gennes, P. G. *J. Phys. (France)* **1981**, *42*, 735.
(4) Watanabe, H. *Prog. Polym. Sci.* **1999**, *24*, 1253.
(5) McLeish, T. C. B. *Adv. Phys.* **2002**, *51*, 1379.
(6) Everaers, R.; Sukumaran, S. K.; Grest, G. S.; Svaneborg, C.; Sivasubramanian, A.; Kremer, K. *Science* **2004**, *303*, 823.
(7) Padding, J. T.; Briels, W. J. *J. Chem. Phys.* **2004**, *120*, 2996.
(8) Harmandaris, V. A.; Mavrantzas, V. G.; Theodorou, D. N.; Kroger, M.; Ramirez, J.; Ottinger, H. C.; Vlassopoulos, D. *Macromolecules* **2003**, *36*, 1376.
(9) Rubinstein, M.; Colby, R. H. *J. Chem. Phys.* **1988**, *89*, 5291.
(10) Warner, M.; Edwards, S. F. *J. Phys. A* **1978**, *11*, 1649.
(11) Rubinstein, M.; Panyukov, S. *Macromolecules* **1997**, *30*, 8036.
(12) Rubinstein, M.; Panyukov, S. *Macromolecules* **2002**, *35*, 6670.
(13) Edwards, S. F.; Vilgis, Th. *Polymer* **1986**, *27*, 483.
(14) Wischnewski, A.; Monkenbusch, M.; Willner, L.; Richter, D.; Likhtman, A. E.; McLeish, T. C. B.; Farago, B. *Phys. Rev. Lett*. **2002**, *88*, 058301.
(15) Wischnewski, A.; Monkenbusch, M.; Willner, L.; Richter, D. *Phys. Rev. Lett*. **2003**, *90*, 058302−1.
(16) Hua, C. C.; Schieber, J. D. *J. Chem. Phys.* **1998**, *109*, 10018.
(17) Shanbhag, S.; Larson, R. G.; Takimoto, J.; Doi, M. *Phys. Rev. Lett.* **2001**, *87*, 195502−1.
(18) Pearson, D. S. et al. *Macromolecules* **1994**, *27*, 711.
(19) Likhtman, A. E.; McLeish, T. C. B. *Macromolecules* **2002**, *35*, 6332.
(20) Fetters, L. J.; Lohse, D. J.; Milner, S. T.; Witten, T. A.; Zirkel, A. *Macromolecules* **1994**, *27*, 4639; and Fetters, L. J.; Lohse, D. J.; Milner, S. T.; Graessley, W. W. *Macromolecules* **1999**, *32*, 6847.
(21) Zamponi, M. et al. In preparation.
(22) Fleischer, G.; Appel, M. *Macromolecules* **1995**, *28*, 7281.
(23) Gotro, J. T.; Graessley, W. W. *Macromolecules* **1984**, *17*, 2767.
(24) Abdel-Goad, M.; Pyckhout-Hintzen, W.; Kahle, S.; Allgaier, J.; Richter, D.; Fetters, L. J. *Macromolecules* **2004**, *37*, 8135.
(25) Fetters, L. J.; Kiss, A. D.; Pearson, D. S.; Quack, G. F.; Vitus, F. J. *Macromolecules* **1993**, *26*, 647.
(26) Richter, D.; Farago, B.; Butera, R.; Fetters, L. J.; Huang, J. S.; Ewen, B. *Macromolecules* **1993**, *26*, 795.
(27) Fatkullin, N.; Kimmich, R. *Phys. Rev. E* **1995**, *52*, 3273.
(28) Colby, R. H.; Fetters, L. J.; Graessley, W. W., *Macromolecules* **1987**, *20*, 2226.
(29) Smith, G. D.; Paul, W.; Monkenbusch, M.; Richter, D. *Chem. Phys.* **2000**, *261*, 61.
(30) Schausberger, A.; Schindlauer, G.; Janeschitz-Kriegl, H. *Rheol. Acta* **1985**, *24*, 220.
(31) Collis, M. W.; Lele, A. K.; Mackley, M. R.; Graham, R. S.; Groves, D. J.; Likhtman, A. E.; Nicholson, T. M.; Harlen, O. G.; McLeish, T. C. B.; Hutchins, L. R.; Fernyhough, C. H.; Young, R. N. *J. Rheol.* **2005**. In press.
(32) de Gennes, P. G. *Physics (Long Island City, NY)* **1967**, *3*, 37.
(33) van Meerveld, J. *Rheol. Acta* **2004**, *43*, 615.

MA050399H